# Full Coulomb calculation of Stark broadened spectra from multielectron ions: A focus on the dense plasma line shift

G. C. Junkel, M. A. Gunderson, and C. F. Hooper, Jr.
*Department of Physics, University of Florida, Gainesville, Florida 32611-8440*

D. A. Haynes, Jr.
*Fusion Technology Institute, University of Wisconsin, Madison, Wisconsin 53706-1687*
(Received 18 February 2000)

Recently, there has been growing experimental evidence for redshifts in line spectra from highly ionized, high-$Z$ radiators immersed in hot, dense plasmas [O. Renner *et al.*, J. Quant. Spectrosc. Radiat. Transf. **58**, 851 (1997); C. F. Hooper *et al.*, in *Strongly Coupled Coulomb Systems* (Plenum, New York, 1998); N. C. Woolsey *et al.*, J. Quant. Spectrosc. Radiat. Transf. **65**, 573 (2000); A. Saemann *et al.*, Phys. Rev. Lett. **82**, 4843 (1999)]. A full Coulomb, multielectron formalism of line broadening due to perturbation by plasma electrons will be presented. A red line shift and asymmetries arise naturally from employing a full Coulomb expression for the perturber-radiator interaction, rather than applying the dipole approximation. This formalism can now be applied to arbitrary multielectron radiating ions.

PACS number(s): 52.25.Nr, 52.25.Ub, 52.58.Ns

## I. INTRODUCTION

In this paper, we continue our efforts to understand the fundamental behavior of plasmas at extreme temperatures and densities [1–3]. A detailed understanding of the interactions of a charged radiator with a plasma environment is needed to characterize hot, dense plasmas such as those generated in implosion experiments using high powered lasers. Recent experiments using the Omega Laser system at the University of Rochester have led us to infer that ionic radiators can experience modifications in their energy-level structure due to deep penetration of the radiator orbitals by plasma electrons [4,5]. These effects are manifested as anomalous broadening and shifting of observed spectral lines. Although spectral line broadening due to plasma ions and electrons has been observed for many years and has been shown to be consistent with existing theories at lower plasma densities, the existence of plasma-induced line shifts has only recently been widely accepted. Presently, the observation of such shifts is established [5–9], and there exist theoretical calculations to predict and explain these shifts for $K$-shell ionic lines [10–12]. The purpose of this article is to present a generalized full Coulomb formalism of line broadening for ionized, multielectron radiators, where the line shifts arise consistently from the relaxation theory. The resulting line-shape calculations contain detailed, angular-momentum-dependent shifts, which lead to substantial line asymmetries. Included in this generalization is the extension of the theoretical capability to shift spectral lines from ionic radiators other than H- and He-like. Spectral-line analysis often results in the study of composite lines, that is, resonance lines together with their accompanying satellites. Since the $K$-shell resonance lines are usually clustered with satellites emitted from ions in He-, Li-, and Be-like configurations, this extension is already necessary in the analysis of dense plasmas where $N_e \approx 10^{24}$ electrons/cm$^3$ and $kT \approx 1$ keV. We have addressed the issue of calculating level shifts for complex configurations and also included intermediate angular-momentum coupling. In the remainder of this introduction, we will briefly highlight some of the history behind plasma-induced line shifts and mention some of the experimental difficulties associated with establishing their existence. Then we will outline a theoretical formalism, focusing on the electron shift and width operator and introducing a generalization for multielectron radiators. In this discussion, the shifts obtained from this formalism will be compared to the theories of Nguyen and Griem and their co-workers. Experimental data will be fitted with theoretical spectra with and without the dense plasma line shift. Finally, possible areas for future study will be considered.

As early as 20 years ago [13,14], interest in spectra of ionized radiators in dense plasmas motivated *ad hoc* calculations of redshifts induced by perturbing the electron shielding of the nucleus. Some early calculations employed linearized Debye-Huckel potentials, while others used self-consistent static charge distributions to describe the shielding of the nucleus [10,11,15–17]. These calculations of what was called the plasma polarization shift frequently overestimated the shifts observed experimentally, particularly those using the Debye-Huckel model. Cooper, Kelleher, and Lee [18] also cautioned against introducing an *ad hoc* shift term in conjunction with the electron broadening operator, pointing out that a shift term should naturally arise as the real part of the broadening operator, while the imaginary part serves to broaden the line shape. In order to obtain consistent result for both line broadening and line shift, Nguyen *et al.* [10] employed a quantum mechanical impact formalism to calculate shift and width terms for Lyman series members of high-$Z$ radiators $\gtrsim 10$. Their calculation included terms of the multipole expansion of the radiator–perturbing-electron interaction, up to the octopole. This is significant because the electron broadening operator was usually calculated in the dipole approximation. These researchers also stated that the monopole term of the interaction contributes the most to the shift, although they did not quantify the extent of this contribution. Also, no attempt was made to calculate line shapes

 

from the results or to present a dynamic, i.e., frequency-dependent shift and width operator. Griem *et al.* [12] then applied a distorted wave scattering approach to the problem, employing perturber wave functions distorted by the monopole term of the radiator–perturbing-electron interaction. This was a first-order impact calculation that summed the phase shifts of the partial waves to obtain the line shifts for He-like Ar. The results were in good agreement (within $\lesssim 15\%$) with those of Ref. [10]. This calculation demonstrated that the bulk of the shift could be obtained by including only the monopole term of the radiator–perturbing-electron interaction potential. Prior to the shift calculations of Hooper *et al.* [5] Griem and his collaborators had been the only ones to incorporate angular-momentum-dependent shifts into actual line-shape calculations.

Although there were shift calculations available for *K*-shell radiators, line shifts due to plasma electron interactions with a radiator had not been incorporated into multielectron line-shape codes such as MERL [2,3] or TOTAL [19]. These codes were written to generate broadened line shapes for the analysis of line spectra of highly charged, multielectron radiators. Improvements have been incorporated recently with respect to radiator interactions with perturbing ions, including ion quadrupole effects and ion dynamics [4,20,21]; however, the reluctance to incorporate shifts into these line broadening calculations was a direct result of the absence of definitive experimental evidence of shifts [13]. Line shifts and shift theories have been difficult to verify experimentally, and only in recent years have data become available that convince us of the existence of line shifts.

In the past, there have been difficulties in measuring line shifts accurately, but recent line-shift observations have confirmed the calculations by Nguyen and Griem and their coworkers. Early experimental verification of shifts observed in spectra emitted from highly charged radiators was partially hindered because most attention was paid to H- and He-like $\alpha$ lines, which we now know experience very small shifts relative to higher lying series members, and which were also most likely to be obscured by opacity effects. Hammel *et al.* [22] measured a redshift in the He $\beta$ line of Ar, $\sim$11 eV at an electron density of $\sim 1.2\times 10^{24}$ cm$^{-3}$, which was roughly consistent with the theories of Nguyen *et al.* and Griem *et al.* and was greater than the instrumental width of their high resolution spectrometer. However, the presence of dielectronic satellites on the red wing complicated the shift measurement and obscured asymmetries arising from the differing shifts of the various angular-momentum states. Leng *et al.* [6] observed small redshifts and a marked asymmetry of the Ly $\gamma$ line of $C^{5+}$. While the bulk shift of the $\gamma$ line seems comparable with those calculated by Nguyen *et al.*, the theoretical line shapes used for fitting were calculated using an average shift, as opposed to incorporating detailed angular-momentum states of the radiator into the initial line-shape calculation, thereby neglecting the asymmetries due to these differing shifts. Further, to account for gradients line shapes were calculated for an expected range of densities and temperatures and summed to form a composite line profile. Both of these approximations would hinder line-shift analysis. Later, Renner *et al.* [7] observed the Lyman series lines of aluminum shift to the red during high resolution flat target experiments. In this case, the density inferences from the widths of the lines relied heavily on the correctness of computer modeling results and cast doubt on the application of any particular shift theory. The difficulties described above allowed the question of the existence of plasma-induced shifts to remain unresolved in the minds of many. In the past few years, more evidence of plasma-induced line shifts has begun to appear. At Lawrence Livermore National Laboratory and the Laboratory for Laser Energetics, in implosion experiments conducted on deuterium filled microballoons, doped with trace amounts of argon, an apparent redshift of the He $\beta$ and He $\gamma$/Lyman $\beta$ complex of *K*-shell Ar was observed, even after satellites were included [4]. Since some of these shifts were far in excess of the experimental error, Hooper *et al.* [5] incorporated a first-order shift calculation for highly ionized radiators into our line-shape code MERL. More recently, Woolsey *et al.* [8] and Saemann *et al.* [9] reported redshifts in the He $\beta$ lines of *K*-shell argon and aluminum, respectively, both roughly consistent with the results of Nguyen *et al.*

Given the accumulation of data supporting the existence of shifts, we now include radiator line shifts due to radiator–plasma-electron interaction as an integral part of our line-shape code; hence, our calculations are consistent and necessitate no adjustable parameters in the spectral analysis. Such an inclusion is important for several reasons. In addition to providing more accurate descriptions of analyzed spectra, this formalism enables us to calculate the shift and width terms simultaneously and self-consistently. Also, we employ a full Coulomb representation of the radiator-perturbing electron interaction, which lends itself to the calculation of not only the first-order monopole term of the multipole expansion but higher order corrections as well. It also has been noted that during high power implosion experiments plasmas are characterized by electron densities where the average electron spacing approaches the size of the radiator orbital. The dipole approximation to the radiator-perturber interaction cannot account for the penetration of such radiator orbitals. Therefore, under these dense plasma conditions, it is inappropriate to apply the dipole approximation to the electron broadening term. In addition to providing shift calculations for H- and He-like radiators, our theory is appropriate to treat cases of multielectron ions, utilizing Cowan's relativistic atomic physics data. The full Coulomb model has been incorporated into our line-shape code MERL, enabling us to generate broadened and shifted line shapes for a greater variety of radiators under a broad range of plasma conditions. In this article, we will limit our discussion to highly ionized radiators in hot, dense plasmas, specifically $Ar^{16+}$ and $Ar^{17+}$ radiators, and their *L*-shell satellite ions, which are immersed in deuterium plasmas characterized by electron densities of $\approx(1\times 10^{23})-(2\times 10^{24})$ cm$^{-3}$ and temperatures between 500 and 2000 eV. Finally, incorporating electron-induced shifts into a model of hot, dense plasmas will, in many cases, have a significant effect on determination of other plasma parameters that are dependent on energy-level structure, such as ionization balance and line-ratio diagnostics.

## II. STARK BROADENING THEORY

Our theoretical development follows standard methods regarding Stark broadening by perturbing electrons and ions.

The current calculation incorporates a model of the plasma that accounts for the motion of the electrons and ions; the latter can have a significant broadening effect at the center of Ar lines when the Ar radiator is immersed in a plasma of relatively lighter ions, such as deuterium, as is the case in inertial confinement fusion implosions. For cases where the ion perturbers are more massive, such as targets filled entirely with higher-$Z$ ions like Ne, Ar, and Kr, ion dynamic effects are reduced greatly and line shapes closely resemble those generated with the static-ion approximation.

We start with the line-shape function given by [23,24]

$$I(\omega)=\frac{4\omega^4}{3c^3}\int_0^\infty d\vec{\mathcal{E}}Q(\vec{\mathcal{E}})J(\omega,\vec{\mathcal{E}}), \tag{1}$$

where $Q(\vec{\mathcal{E}})$ is the ion microfield probability distribution function and $J(\omega,\vec{\mathcal{E}})$ is defined as

$$J(\omega,\vec{\mathcal{E}})=-\frac{1}{\pi}\mathrm{Re}\,\mathrm{Tr}_r[\mathbf{d}\cdot R(\omega,\vec{\mathcal{E}})\rho_r\mathbf{d}]. \tag{2}$$

$J(\omega,\vec{\mathcal{E}})$ is the electron-broadened line profile for a radiating ion in the presence of the ion microfield $\vec{\mathcal{E}}$. $\mathrm{Tr}_r$ is a trace over the relevant radiator states, $\mathbf{d}$ is the radiator dipole operator, and $\rho_r$ is the density matrix for those radiator states. In Eq. (1), Doppler broadening of the line shape due to radiator motion is included at the end of the calculations by convolving $I(\omega)$ with a Doppler profile based on a Maxwellian velocity distribution [1]. The resolvent, $R(\omega,\vec{\mathcal{E}})$ is given by [4,21]

$$R(\omega,\vec{\mathcal{E}})=\frac{G(\Delta\omega,\vec{\mathcal{E}})}{1+i\nu(\Delta\omega)\int d\vec{\mathcal{E}}'Q(\vec{\mathcal{E}}')G(\Delta\omega,\vec{\mathcal{E}}')}, \tag{3}$$

$$G(\Delta\omega,\vec{\mathcal{E}})=\frac{1}{\Delta\omega-L_{i,r}(\vec{\mathcal{E}})-B-M(\Delta\omega)-i\nu(\Delta\omega)}. \tag{4}$$

$\Delta\omega=(\omega-L_r)$, where $L_r$ is the Liouville operator associated with the unperturbed Hamiltonian of the radiator; $L_{i,r}(\vec{\mathcal{E}})$ incorporates the interaction of the radiator with the ion microfield. The quantity $\nu(\Delta\omega)$ is a measure of the effects of perturber ion motion on the radiator, and can be thought of as an effective collision frequency. If $\nu(\Delta\omega)$ is allowed to go to zero, the expressions above reduce to the static-ion approximation. The sum of $B$ and $M(\Delta\omega)$ includes the effects of the plasma electrons on the radiator. We will discuss these two terms in the following section.

### III. RELAXATION MODEL OF ELECTRON BROADENING

In order to comment further on the operators $B$ and $M(\Delta\omega)$, we first write the Hamiltonian $H'$ in which the effects of the radiator–perturbing-ion interaction have already been incorporated into the ion microfield:

$$H'=H_r+e\mathcal{E}Z_r+K_e+V_{er}+V_{ee}. \tag{5}$$

The first term on the right hand side is the Hamiltonian for an isolated radiator. In the second term, the effects of the perturbing ions have been expressed in terms of the radiator dipole interacting with the ion microfield. It may seem counterintuitive to suggest that the dipole approximation is valid for radiator interactions with plasma ions, but invalid for interactions with plasma electrons at high densities. However, for highly charged radiators, the perturbing ions experience a strong repulsion due to the monopole interaction with the radiator, which is included in the microfield calculation. Therefore, the ions remain sufficiently distant from the radiator for the dipole approximation to be valid. Higher order corrections to the dipole approximation have been evaluated and appear to have a relatively small effect for the plasma conditions considered here [20]. This is not the case for plasma electrons, which experience an equally strong attraction and may have the opportunity to penetrate the radiator orbitals. Continuing with the rest of the Hamiltonian, $K_e$ is the kinetic energy of the plasma electrons, $V_{er}$ is the radiator–perturbing-electron interaction, and $V_{ee}$ represents the perturbing-electron–electron interactions. In order to calculate $B$ and $M(\Delta\omega)$, the interaction potential between the radiator and a given plasma electron is divided into a long-range monopole term $V^{(0)}(j)$ and a short-range interaction $V^{(1)}(r,j)$ as follows, where $V^{(0)}(j)$ is the monopole interaction of the $j$th perturbing electron with the radiator and $x_j$ is the coordinate of that electron:

$$V^{(0)}(j)=-\frac{(Z-N_r)}{x_j}, \tag{6}$$

$$V^{(1)}(r,j)=\left(\frac{1}{|x_j-x_{r_1}|}-\frac{1}{x_j}\right)+\left(\frac{1}{|x_j-x_{r_2}|}-\frac{1}{x_j}\right)+\cdots+\left(\frac{1}{|x_j-x_{r_{N_r}}|}-\frac{1}{x_j}\right). \tag{7}$$

The remaining interaction $V^{(1)}(r,j)$ is expressed as a sum of interactions with the $N_r$ individual radiator electrons. The coordinates of the $i$th radiator electron are denoted by $x_{r_i}$. Later, we will take advantage of the fact that $V^{(1)}(r,j)$ has been expressed as a sum of symmetric operators on the radiator electron coordinates. $V^{(0)}(j)$ is independent of radiator electron coordinates and may be included in the Hamiltonian of the plasma electrons,

$$H(j)=\frac{p_j^2}{2m}-V^{(0)}(j). \tag{8}$$

This form lends itself to employing Coulomb wave functions to describe the motion of the perturbing electrons, as was done in the past [1,25]. We can now define Liouville operators $L(r,1)$ and $L_1(r,1)$, as follows:

$$L(r,1)\hat{f}=[H'(r,1),\hat{f}],\quad L_1(r,1)\hat{f}=[V^{(1)}(r,1),\hat{f}], \tag{9}$$

where $\hat{f}$ is an arbitrary operator. $H'(r,1)$ represents the Hamiltonian for the radiator interacting with the ion microfield and a single plasma electron:

$$H'(r,1)=H_r+e\mathcal{E}Z_r+H(1)+V^{(1)}(r,1). \tag{10}$$

Using kinetic theory techniques, the electron interaction operators $B$ and $M(\Delta\omega)$ can be expressed in terms of $L(r,1)$ and $L_1(r,1)$ [25–27]:

$$B = n \,\mathrm{Tr}_1 \, L_1(r,1) f(r,1) f(r)^{-1}, \tag{11}$$

$$M(\omega) = n \,\mathrm{Tr}_1 \{ \mathcal{L}_1(r,1;\omega) [\omega - L(r,1) - V(r,1;\omega)]^{-1} \times f(r,1) \mathcal{L}_1(r,1) f(r)^{-1} \}, \tag{12}$$

where $f(r)$ and $f(r,1)$ are distribution functions for the isolated radiator and the radiator–perturbing-electron system, respectively. $\mathcal{L}_1(r,1;\omega)$ and $\mathcal{L}_1(r,1)$ are simply dynamically and statically shielded forms of $L_1(r,1)$. $V(r,1;\omega)$ incorporates the effects of other plasma electrons on the radiator-perturber system. The frequency-independent term $B$ represents the time-independent portion of the interaction of the plasma electrons with the radiator. It is real and provides the bulk of the shift. $M(\omega)$ is the transform of the autocorrelation function of the electron interaction potential. At this point, $B$ and $M(\omega)$ are exact to all orders in the radiator–plasma-electron interaction potential.

As has been argued in the past [28,29,12], we will calculate these terms to second order in the radiator–perturbing-electron interaction $L_1(r,1)$, using a full Coulomb expression of the interaction potential. The second-order approximation is an appropriate choice for two reasons. First of all, large portions of the $\alpha$, $\beta$, and $\gamma$ lines of $K$-shell Ar, for the plasma conditions under consideration, satisfy the inequality $\Delta\omega \lesssim 2\omega_{pe}$, where $\Delta\omega$ is the frequency separation from line center and $\omega_{pe}$ is the plasma frequency. This is relevant because second-order calculations have been shown to be valid in this range [29]. Second, in order to truncate the expansion of the shift and width operators at second order in the interaction potential, the perturbing electrons must undergo only collisions that are weak in the sense that the transfer of momentum is small compared to the perturber momentum; that is to say, the impulse experienced by the perturber is small. The change in momentum can be related to the potential experienced by the perturber at the point of closest approach, $V = eZ^*/r_{min}$. Since the plasmas under consideration are characterized by sufficiently high temperatures, even collisions where the perturbing electron penetrates the bound electron orbital can be described as ''weak.'' The appropriate temperature regime was defined, for a hydrogenic radiator, with the expressions [18]

$$mv\,\delta v \sim \frac{e^2(Z-1)}{r_{min}}, \tag{13}$$

$$\frac{mv\,\delta v}{mv^2} \sim \frac{e^2(Z-1)Z}{a_0 n^2 kT} \ll 1, \tag{14}$$

$$kT > \frac{Z(Z-1)}{n^2}\,\mathrm{Ry}, \tag{15}$$

where $Z$ is the radiator charge and $n$ is the principal quantum number of the radiator state. At higher temperatures, the average plasma electron has a greater kinetic energy and spends a relatively short time near the radiator itself and can thus receive only a small impulse, relative to its momentum.

Given the conditions described above, it has been shown that $B$, the static shift, can be expanded into two terms $B^{(1)}$ and $B^{(2)}$, which are first and second order in the interaction potential, respectively [30]. We can expand the distribution function $f(r,1)$, and thus $B$, in terms of $V^{(1)}(r,1)$. By successively closing kinetic equations in the equilibrium Bogoliubov-Born-Green-Kirkwood-Yvon hierarchy, Dufty and Boercker obtained an expression for $f(r,1)$ [27]:

$$f(r,1) = Z \exp\{-\beta[H(r) + H(1) + V_s(r,1)]\}, \tag{16}$$

where $V_s(r,1)$ is a statically screened radiator-electron interaction potential. Boercker and Iglesias expanded $f(r,1)$ in orders of $V_s(r,1)$ and obtained the following expressions for $B^{(1)}$ and $B^{(2)}$ [30]:

$$B^{(1)} = n \,\mathrm{Tr}_1 [L_1(r,1) f_0(1)], \tag{17}$$

$$B^{(2)} = -n \,\mathrm{Tr}_1 \left( L_1(r,1) f_0(r) f_0(1) \int_0^\beta d\tau e^{\tau[H(r)+H(1)]} \times V_s(r,1) e^{-\tau[H(r)+H(1)]} f_0(r)^{-1} \right). \tag{18}$$

Starting with Eqs. (17) and (18), we can express the trace over perturber states in terms of integrals over perturber momenta. Then, we introduce complete sets of radiator eigenstates to obtain a matrix representation in Eqs. (19) and (20). Finally, we evaluate the integral over $\tau$. Although $B^{(1)}$ and $B^{(2)}$ are tetradic operators, we have shown only the direct term of $B^{(1)}$. There is an interference term, which we can neglect if we assume that there are no nonradiative transitions between initial and final states. It should be noted that there are no corresponding direct or interference terms for the lower states for $B^{(2)}$, although such terms are found in the dynamic term $M(\Delta\omega)$.

$$B^{(1)}_{ifi'f'} = n\lambda_T^3 \int d\mathbf{k} e^{-\beta k^2} \langle i\mathbf{k}|V^{(1)}(r,1)|i'\mathbf{k}\rangle \delta_{ff'} - \langle f\mathbf{k}|V^{(1)}(r,1)|f'\mathbf{k}\rangle \delta_{ii'}, \tag{19}$$

$$B^{(2)}_{ifi'f'} = -n\lambda_T^3 \int d\mathbf{k}_1 \int d\mathbf{k}_2 \sum_{i''} \frac{(e^{-\beta k_1^2} - e^{-\beta(k_2^2 + \omega_{i''} - \omega_{i'})})}{(\omega_{i''} - \omega_{i'} + k_2^2 - k_1^2)} \times \langle i\mathbf{k}_1|V^{(1)}(r,1)|i''\mathbf{k}_2\rangle \langle i''\mathbf{k}_2|V_s(r,1)|i'\mathbf{k}_1\rangle \delta_{ff'}. \tag{20}$$

Returning to Eq. (12), we see that $M(\omega)$ is already at least second order in $L_1(r,1)$, so that we should replace $[\omega - L(r,1) - V(r,1;\omega)]^{-1}$ with $[\omega - L(r) - L(1)]^{-1}$. In the form presented below, the term $M(\Delta\omega)_{i,i'}$, which describes the interaction of the initial states, is reexpressed as an integral over time. There is a corresponding term for the interaction of the final states.

$$M(\omega)_{ii'} = -in\lambda_T \int d\mathbf{k}_1 \int d\mathbf{k}_2 \int dt \sum_{i''} e^{-\beta k_2^2} \times e^{i(\Delta\omega_{i''f} + k_1^2 - k_2^2 + i\epsilon)t} \times \langle i\mathbf{k}_1|V_s(r,1)|i''\mathbf{k}_2\rangle \times \langle i''\mathbf{k}_2|V_s(r,1)|i'\mathbf{k}_1\rangle \delta_{f'f}. \tag{21}$$

Boercker and Iglesias showed for *neutral* radiators that there is significant cancellation in the portion of the shift term that is second order in the interaction potential, between $B^{(2)}$ and $\mathrm{Re}\,M(\omega)$. This is important for the neutral case, where the first-order term is believed to vanish [30]. It can be shown that the second-order behavior is qualitatively the same for charged radiators; however, the resulting cancelation is a relatively small effect for highly charged radiators, since the first-order shift is dominant.

So far, our expressions have not specified the details of the interaction. In the next section, we will address the challenges of calculating the matrix element $\langle i,\mathbf{k}_1|V^{(1)}(r,1)|i'\mathbf{k}_2\rangle$ for a multielectron radiator.

## IV. MULTIELECTRON FORMALISM

In Eqs. (20) and (21), the ket $|i,\mathbf{k}\rangle$ represents a direct product of the energy eigenstates for the radiator and perturbing electron. However, matrix elements of the interactions are easiest to calculate in the LS representation of coupled angular momentum states using Slater determinants of product wave functions for the radiator electrons. Some multielectron atoms and ions can experience intermediate coupling between angular-momentum states; hence, in order to calculate the matrix elements of the interactions, it is necessary to first transform from the energy eigenstates to specific electron configurations in the LS representation. A transformation matrix can be obtained by diagonalizing the matrix of the isolated radiator Hamiltonian but retaining the eigenvectors for the particular representation most useful for the model. An example of such a matrix is given in Table 10-2 in Ref. [31]. Since Cowan does not provide a specific notation for this operator, we shall refer to it as $\mathbf{T}_{\alpha,i}$. The subscript $\alpha$ refers to all the relevant quantum numbers, except $\mathcal{J}$ and $\mathcal{M}$, which represent the total angular momentum and its azimuthal component, of a given configuration in the appropriate representation; in this case, we employ the genealogical LS basis. This representation is described in Sec. 4.10 of Ref. [31]. We note that for an isolated radiator the potential is spherically symmetric, and the total angular momentum is conserved. Therefore, $\mathbf{T}_{\alpha,i}$ is block diagonal in $\mathcal{J}$ and invariant in $\mathcal{M}$. We will designate individual blocks by $\mathbf{T}_{\alpha,i}(\mathcal{J})$ and the relevant basis states by $|\Psi_\alpha\rangle_{\mathcal{J}\mathcal{M}}$. Therefore, the $i$th wave function $|i\rangle_{\mathcal{J}\mathcal{M}}$ in the energy basis can be expressed as

$$|i\rangle_{\mathcal{J}\mathcal{M}}=\sum_\alpha |\Psi_\alpha\rangle_{\mathcal{J}\mathcal{M}}\mathbf{T}_{\alpha,i}(\mathcal{J}), \tag{22}$$

which results in the following matrix elements of the radiator–perturbing-electron interaction:

$$\begin{aligned}{}_{\mathcal{J}\mathcal{M}}\langle i;\mathbf{k}_1|V_s(r,1)|i';\mathbf{k}_2\rangle_{\mathcal{J}'\mathcal{M}'} &= \sum_{\alpha,\alpha'} \mathbf{T}^\dagger_{i,\alpha}(\mathcal{J})_{\mathcal{J}\mathcal{M}} \\ &\times\langle\Psi_\alpha;\mathbf{k}_1|V_s(r,1)|\Psi_{\alpha'};\mathbf{k}_2\rangle_{\mathcal{J}'\mathcal{M}'} \\ &\times\mathbf{T}_{\alpha',i'}(\mathcal{J}').\end{aligned} \tag{23}$$

In order to calculate the matrix elements of the interaction, it is important to remember that $V^{(1)}(r,1)$ was defined in Eq. (7) as a sum of symmetric, one-electron operators. This allows us to employ tools described in detail by Cowan [31]. The first step is to express our interaction in terms of reduced matrix elements. $V^{(1)}(r,1)$ can be expressed as a multipole expansion in terms of reduced tensor operators for each radiator electron coordinate $x_{r_j}$,

$$V^{(1)}(r_j,1)=\sum_{t=0}^{\infty}\sum_{q=-t}^{t} V^t(x_{r_j},x_1)C_q^{(t)}(\hat{x}_{r_j})C_q^{(t)\dagger}(\hat{x}_1), \tag{24}$$

where $V^t$ and $C_q^{(t)}$ describe the radial and angular portions of the multipole expansion,

$$V_j^t=\left(\frac{x_<^t}{x_>^{t+1}}-\frac{\delta_{t,0}}{x_1}\right),\quad C_q^{(t)}(\theta,\phi)\equiv\left(\frac{4\pi}{2t+1}\right)^{1/2}Y_{tq}(\theta,\phi). \tag{25}$$

Here $x_1$ is the plasma electron coordinate, and $x_<$ and $x_>$ are the lesser and greater, respectively, of the perturbing electron coordinates and relevant radiator electron coordinates. In order to account for screening due to electron correlations, we will follow the usual practice of introducing a cutoff at the Debye radius when we integrate over the perturbing electron coordinates. This choice allows us to compare our results more easily with the many other calculations that employed this cutoff. In our next step, we employ the Wigner-Eckart theorem to obtain reduced matrix elements. We also reexpress our perturber wave functions in terms of a partial wave expansion:

$$\begin{aligned}{}_{\mathcal{J}\mathcal{M}}\langle\Psi_\alpha;\mathbf{k}_1|V_s(r,1)|\Psi_{\alpha'};\mathbf{k}_2\rangle_{\mathcal{J}'\mathcal{M}'} &= \sum_{l_1,m_1}\sum_{l_2,m_2}\sum_{t,q}(-1)^{\mathcal{J}-\mathcal{M}+l_1-l_1+q} \\ &\times\begin{pmatrix}\mathcal{J} & t & \mathcal{J}'\\ -\mathcal{M} & q & \mathcal{M}'\end{pmatrix}\begin{pmatrix}l_1 & t & l_2\\ -m_1 & -q & m_2\end{pmatrix} \\ &\times\left\langle\Psi_{\alpha,\mathcal{J}};k_1,l_1\left|\left|\sum_{j=1}^{N_r}V_j^tC_j^{(t)}C_1^{(t)\dagger}\right|\right|\Psi_{\alpha',\mathcal{J}'};k_2,l_2\right\rangle.\end{aligned} \tag{26}$$

The expression

$$\langle\Psi_{\alpha,\mathcal{J}};k_1,l_1||\Sigma_jV_j^tC_j^{(t)}C_1^{(t)}||\Psi_{\alpha',\mathcal{J}'};k_2,l_2\rangle$$

is independent of the magnetic quantum numbers $m$ and $\mathcal{M}$ and the index $q$; it is also analogous to that used by Cowan to calculate general transition arrays. This matrix element can be expressed in terms of single-electron interactions. This is achieved by employing a tedious but tractable process of accounting for coordinate permutations, coefficient of fractional parentage expansions, and uncoupling or recoupling angular momenta, which Cowan denotes with the operators $D_1$ through $D_7$. One may refer to the Appendix for more details. Here, we show only an abbreviated form similar to Eq. (14.78) in [31]:

$$\left\langle \Psi_{\alpha,\mathcal{J}};k_1,l_1\left|\left|\sum_{r=1}^{N_r} V_r^t C_r^{(t)} C_1^{(t)}\right|\right|\Psi_{\alpha',\mathcal{J}'};k_2,l_2\right\rangle$$
$$=\langle k_1,l_1||D_1D_2D_3\cdots D_7\langle n_i,l_i||V^tC^{(t)}||n_j,l_j\rangle \times C_1^{(t)}||k_2,l_2\rangle$$
$$=\langle k_1,l_1||\mathbf{A}^{(t)}_{\alpha,\alpha'}(x_1)C_1^{(t)}||k_2,l_2\rangle, \tag{27}$$

where

$$\mathbf{A}^{(t)}_{\alpha,\alpha'}(x_1)=D_1D_2D_3\cdots D_7(-1)^{l_i}[l_i,l_j]^{1/2}\begin{pmatrix} l_i & t & l_j \\ 0 & 0 & 0\end{pmatrix} \times\int dx_r x_r^2 R^*_{n_i,l_i}(x_r)\left(\frac{x_<^t}{x_>^{t+1}}-\frac{\delta_{t,0}}{x_1}\right)R_{n_j,l_j}(x_r). \tag{28}$$

The indices $i$ and $j$ refer to the subshells relevant to the one-electron transition. The quantity $\mathbf{A}^{(t)}_{\alpha,\alpha'}(x_1)$ in Eq. (28) is an expression for the matrix element of the $t$th term in the multipole expansion of the interaction $V^{(1)}(r,1)$, integrated over the radiator state of a single bound electron. $R_{n,l}(x_r)$ is the relativistic wave function of the bound electron extracted from Cowan's atomic physics code. Now we can express $B$ and $M(\Delta\omega)$ in more familiar forms by replacing the perturber states with Coulomb wave functions $F_l(\eta,kx_1)$, where $l$ is the quantum number representing the angular momenta in the partial wave expansion and $k$ is the wave number of the perturber momentum:

$$B^{(1)}_{ifi'f'}=\frac{2}{\pi}n\lambda_T^3\sum_{\alpha,\alpha'}\sum_{t=0}^{\infty}\sum_{l=0}^{\infty}\delta_{t,0}\delta_{\mathcal{M},\mathcal{M}'}\delta_{\mathcal{J},\mathcal{J}'}\delta_{ff'} \times\int dk\, e^{-\beta k^2}(2l+1)\times\mathbf{T}^{\dagger}_{i,\alpha}(\mathcal{J})\int dx_1 F_l(\eta,kx_1) \times\mathbf{A}^t_{\alpha\alpha'}(x_1)F_l(\eta,kx_1)\mathbf{T}_{\alpha',i'}(\mathcal{J})-B^{(1)}_{ff'}\delta_{ii'}. \tag{29}$$

Note that only the penetrating monopole term contributes to $B^{(1)}$, even for the multi-electron case. Let us define the operator $D_{i,i'',i'}(k_1,k_2)$ so that we have simplified expressions for $B^{(2)}$ and $M(\Delta\omega)$:

$$D_{i,i'',i'}(k_1,k_2)=\sum_{\substack{\alpha,\alpha'\\ \alpha'',\alpha'''}}\sum_{t=0}^{\infty}\sum_{l_1,l_2}(-1)^{\mathcal{J}+\mathcal{J}''}\frac{(2l_1+1)(2l_2+1)}{(2t+1)(2\mathcal{J}+1)} \times\begin{pmatrix} l_1 & t & l_2 \\ 0 & 0 & 0\end{pmatrix}^2\delta_{\mathcal{J},\mathcal{J}'}\delta_{\mathcal{M},\mathcal{M}'}\mathbf{T}^{\dagger}_{i,\alpha}(\mathcal{J}) \times\int dx\, F_{l_1}(\eta_1,k_1x)\mathbf{A}^{(t)}_{\alpha,\alpha''}(x)F_{l_2}(\eta_2,k_2x) \times\mathbf{T}_{\alpha'',i''}(\mathcal{J}'')\mathbf{T}^{\dagger}_{i'',\alpha'''}(\mathcal{J}') \times\int dx' F_{l_2}(\eta_2,k_2x')\mathbf{A}^{(t)}_{\alpha''',\alpha'}(x') \times F_{l_1}(\eta_1,k_1x')\mathbf{T}_{\alpha',i'}(\mathcal{J}). \tag{30}$$

This leads us to

$$B^{(2)}_{ifi'f'}=-\frac{4n\lambda_T^3}{\pi^2}\int dk_1\int dk_2\sum_{i''}\frac{(e^{-\beta k_1^2}-e^{-\beta(k_2^2+\omega_{i''}-\omega_{i'})})}{(\omega_{i''}-\omega_{i'}+k_2^2-k_1^2)} \times D_{i,i'',i'}(k_1,k_2)\delta_{ff'}, \tag{31}$$

$$M(\Delta\omega)_{ii'}=-i\frac{4n\lambda_T^3}{\pi^2}\int dk_1\int dk_2\int dt\sum_{i''}e^{-\beta k_2^2} \times e^{i(\Delta\omega_{i''f}+k_1^2-k_2^2+i\epsilon)t}D_{i,i'',i'}(k_1,k_2)\delta_{ff'}. \tag{32}$$

While the quantities, $B^{(1)}$ and $B^{(2)}$ are real and contribute only to the shift, the dynamic term $M(\Delta\omega)$ is complex. It contributes to both the shift and the width. If we take the integral over time, we get the following expressions:

$$\mathrm{Re}\,M(\omega)_{ii'}$$
$$=\begin{cases}\dfrac{4n\lambda_T^3}{\pi^2}\displaystyle\sum_{i''}\mathrm{P}\int dk_1\int dk_2\left(\Delta\omega_{i''f}+\frac{\hbar}{2m}(k_1^2-k_2^2)\right)^{-1}\left[e^{-\beta\hbar^2k_2^2/2m}D_{i,i'',i'}(k_1,k_2)-e^{-\beta(\hbar^2k_1^2/2m+\hbar\Delta\omega_{i''f})}D_{i,i'',i'}\left(k_1,\left(k_1^2+\frac{2m\Delta\omega_{i''f}}{\hbar}\right)^{1/2}\right)\right], & \Delta\omega_{i''f}>0 \quad (33)\\ \dfrac{4n\lambda_T^3}{\pi^2}\displaystyle\sum_{i''}\mathrm{P}\int dk_1\int dk_2\left(\Delta\omega_{i''f}+\frac{\hbar}{2m}(k_1^2-k_2^2)\right)^{-1}e^{-\beta\hbar^2k_2^2/2m}\left[D_{i,i'',i'}(k_1,k_2)-D_{i,i'',i'}\left(\left(k_2^2+\frac{2m|\Delta\omega_{i''f}|}{\hbar}\right)^{1/2},k_2\right)\right], & \Delta\omega_{i''f}<0, \quad (34)\end{cases}$$

$$\mathrm{Im}\,M(\omega)_{ii'}=\begin{cases}-\dfrac{4n\lambda_T^3}{\pi^2}\dfrac{m\pi}{\hbar}\displaystyle\sum_{i''}\int dk_1 e^{-\beta(\hbar^2k_1^2/2m+\hbar\Delta\omega_{i''f})}\frac{D_{i,i'',i'}(k_1,(k_1^2+2m\Delta\omega_{i''f}/\hbar)^{1/2})}{(k_1^2+2m\Delta\omega_{i''f}/\hbar)^{1/2}}, & \Delta\omega_{i''f}> \quad (35)\\ -\dfrac{4n\lambda_T^3}{\pi^2}\dfrac{m\pi}{\hbar}\displaystyle\sum_{i''}\int dk_2 e^{-\beta(\hbar^2k_2^2/2m)}\frac{D_{i,i'',i'}((k_2^2+2m|\Delta\omega_{i''f}|/\hbar)^{1/2},k_2)}{(k_2^2+2m|\Delta\omega_{i''f}|/\hbar)^{1/2}}, & \Delta\omega_{i''f}<0. \quad (36)\end{cases}$$

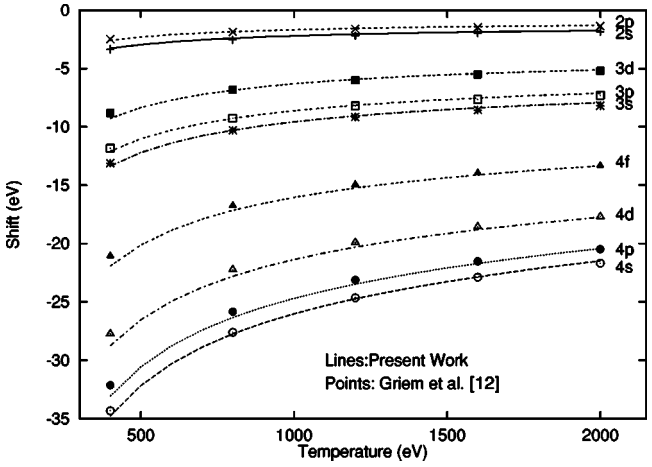


FIG. 1. Comparison of shifts, first order in the interaction potential, of helium-like Ar with shift calculations by Griem *et al.* [12]; electron density $1\times10^{24}$ cm$^{-3}$. Note the increase in the magnitude of the level shifts with increasing principal quantum number.

## V. RESULTS

In this section, we will present the results of our calculations using the full Coulomb, multielectron formalism. First, in Fig. 1 we see the first-order shift $B^{(1)}$ as a function of temperature for $Ar^{16+}$ immersed in a plasma characterized by an electron density $N_e=1\times10^{24}$ cm$^{-3}$. From Eq. (17), we see that that the shift is linear in density, excepting small effects due to plasma electron correlations. Also in Fig. (1), the first-order shift is shown to be in good agreement with the calculation of Griem *et al.* [12]. It is apparent that the shift is strongly dependent on the initial states of the radiator, particularly its principal quantum number $n$. This is consistent with the difficulty experienced in measuring the shift of lower lying lines, such as the $\alpha$ or $\beta$ lines, where the shift is often less than the instrumental resolution. The effect of increasing shift with increasing principal quantum number may cause difficulties when calculating lines in a Rydberg series. One can anticipate, at sufficiently high electron densities, higher lying lines shifting past their lower $n$ neighbors, if the linear dependence is valid for such high densities. However, the magnitudes of nonzero, off-diagonal matrix elements of the first-order shift $B^{(1)}$ are on the order of the diagonal elements. For example, the element $B^{(1)}_{4p,5p}$ is about $B^{(1)}_{4p,4p}$. In preliminary calculations we have shown that mixing between states within a Rydberg series, due to interactions with perturbing electrons *and* ions, tends to cause the spectral lines not to pass one another, but to ''pile up'' against one another. This phenomenon, as well as the effects of the plasma-induced shift on the ionization balance, will be addressed in subsequent articles.

The differing shifts of the angular momentum states can result in a distinct asymmetry of the line profile, as well as a shift. Figures 2(a) and 2(b) show profiles of the He $\beta$ and He $\gamma$ lines of $Ar^{16+}$ as a function of temperature for $N_e=1\times10^{24}$ cm$^{-3}$. Notice the more pronounced asymmetry of the shifted line shapes at lower temperatures. While the shift, as a whole, is weakly dependent on the temperature, the profile shape is more strongly dependent on temperature than line profiles calculated in the dipole approximation, as seen in Figs. 3(a) and 3(b). Although the lines represent $1s3p$-$1s^2$ and $1s4p$-$1s^2$ transitions, respectively, the mixing of the radiator states due to the ion microfield allows asymmetries to arise. This is especially true for states with higher angular momenta. For example, although the center of mass of the line profile of He $\gamma$ shifts approximately at the rate of the $1s4p$-$1s^2$ transition, the ''peak'' shifts less, reflecting the mixing with the higher angular-momentum states. This will result in an underestimation of the shift, if one only measures the shift of the peak.

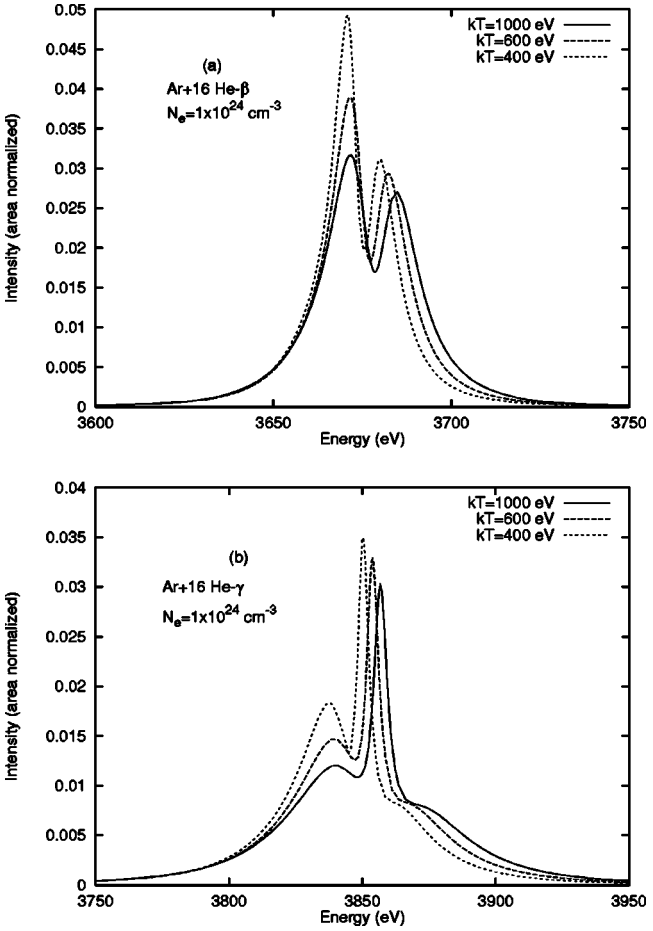


FIG. 2. Comparison of broadened line shapes using a full Coulomb expression for the radiator–perturbing-electron interaction. The $Ar^{16+}$ He $\beta$ and He $\gamma$ lines are shown as a function of temperature, with an electron density $N_e=1\times10^{24}$ cm$^{-3}$. The shift in the full Coulomb calculation causes increasing distortion as the temperature decreases.

Although a line may also experience asymmetries due to quadrupole interactions of the radiator with gradients of the ion microfield, this effect is less than 10% of the asymmetry due to the electron shift. Also, any asymmetries due to mixing between bound radiator manifolds is negligible at the densities under consideration ($\lesssim10^{24}$ cm$^{-3}$).

In order to confirm the validity of terminating the perturbation expansion of the shift and width operator at second order in the radiator–perturbing-electron interaction, line shapes using the current formalism were compared to those calculated with an all-order, semiclassical formalism that is presently under development [32–35]. In the electron density and temperature regime relevant to high power laser implosions, there is good agreement between the two models.

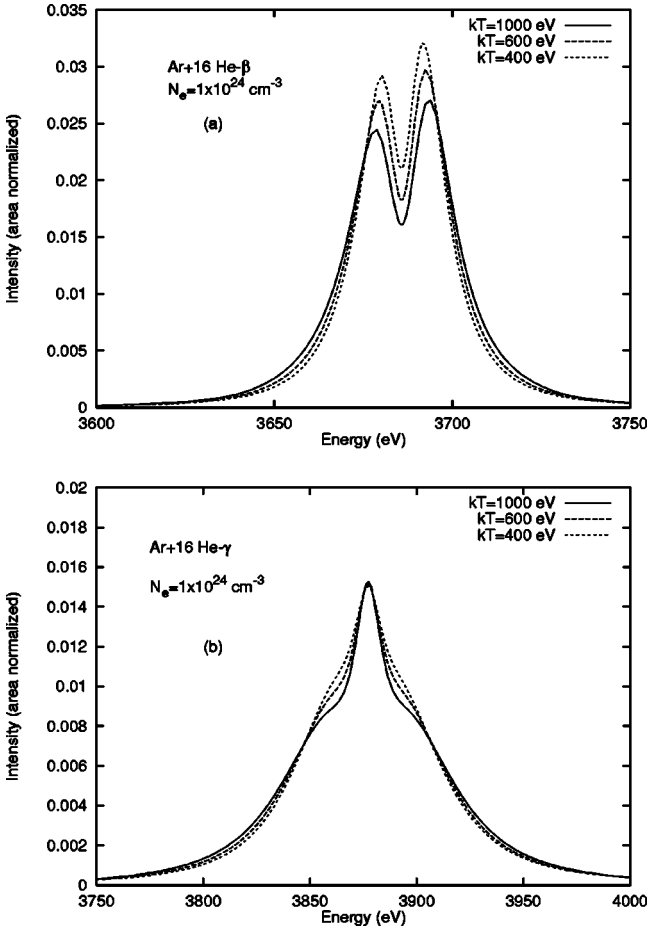


FIG. 3. The $Ar^{16+}$ He $\beta$ and He $\gamma$ lines, calculated in the dipole approximation of the radiator–perturbing-electron interaction, are shown as a function of temperature, with an electron density $N_e = 1\times10^{24}$ cm$^{-3}$. There are no shifts or asymmetries in the line shapes, and the temperature dependence is not as pronounced as is seen in Figs. 2(a) and 2(b).

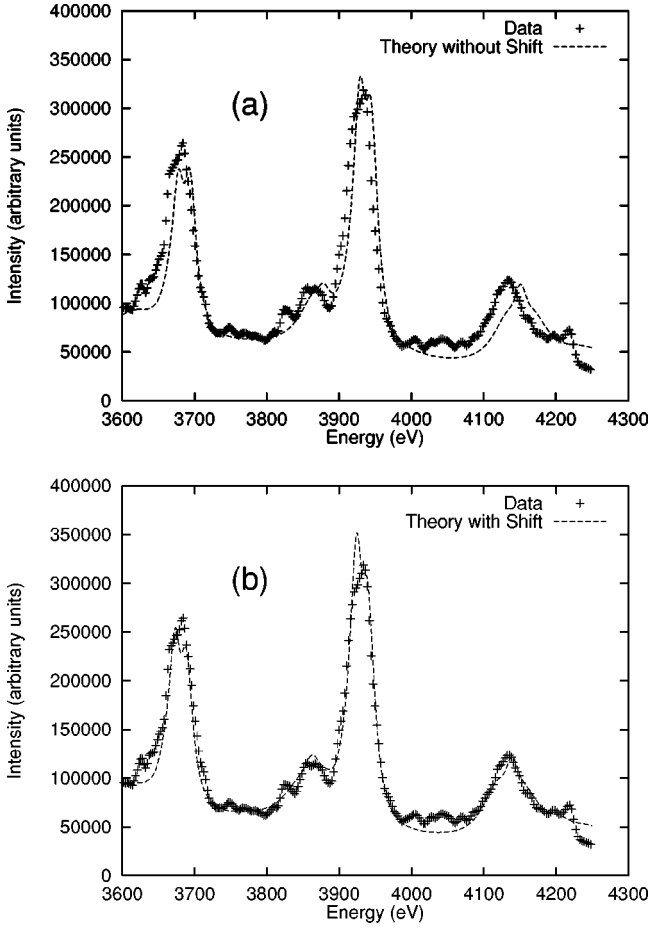


FIG. 4. Comparison of a time-resolved Ar *K*-shell spectrum with calculated spectra with (a) unshifted line shapes and (b) shifted line shapes for $n_e = 9\times10^{23}$ cm$^{-3}$, $kT = 1350$ eV. The spectrum was recorded over a 30 ps period during a laser-driven microballoon implosion experiment where the $D_2$ fuel was doped with 0.125% Ar. Edge effects on the data due to the photocathode can be seen just to the right of the Lyman $\gamma$ line, where the spectrum seems to drop off rapidly.

Using theoretical line shapes that include shifts allows significant improvements in the interpretation of experimental data. Time-resolved Ar *K*-shell (3–4.5 keV) spectra were obtained during microballoon implosions performed using the OMEGA laser system at the Laboratory for Laser Energetics at the University of Rochester [36]. 20 $\mu$m thick plastic microballoons of 440 $\mu$m inner radius were filled with 20 atm of deuterium doped with 0.25% Ar. The microballoons were imploded by 20–25 kJ of ultraviolet energy distributed symmetrically among 60 beams. Time-resolved Ar x-ray line spectra were used to characterize the plasma during the implosion. The spectra were recorded using a streaked spectrograph with a rubidium acid phthalate (RbAP) crystal dispersing the spectrum onto a 250 Å Au photocathode. Spectral and temporal resolution were approximately $E/\Delta E \approx 500$ and $\Delta t \approx 20-30$ ps, respectively. The resulting images were recorded on film, then digitized. Verifying the presence of shifts first requires careful determination of the isolated-ion line position; the digitized images were corrected for film sensitivity and known streak-camera-induced distortions including streak angle and curvature of isotemporal lines [37]. The wavelength dispersion was determined from the line positions at early time, when the low densities assured negligible shifts. This same dispersion was then used for all times.

Before comparing the theoretical spectrum with experimental data, steps were taken to account for (1) shell opacity, (2) filtering, (3) Au photocathode response, and (4) the instrumental response function due mainly to source size broadening. No arbitrary, wholesale shift of the theoretical spectrum was permitted, and thus the theoretical line positions were those obtained using Cowan's [31] atomic physics suite as input into our spectral line profile calculation.

In order to analyze the data, theoretical spectra were calculated using the following lines: Ar He $\beta$ ($1s3l \rightarrow 1s^2$), He $\gamma$, He $\delta$, Ly $\beta$, Ly $\gamma$, Ly $\delta$, and attendant satellites of He $\beta$, He $\gamma$, and Ly $\beta$. It is important to include satellites since their appearance in the spectra can be incorrectly interpreted as broadening and shifting of the resonance lines. We employed line shapes corresponding to a single temperature and density. While temperature and density gradients do occur in implosion experiments, LILAC simulations at the University of Rochester indicate that for these cases gradients are small. In fact, we have had success fitting lines from such implosions with a single temperature and density for time intervals of ~20 ps. The relative intensities of the lines were calcu-

lated using a nonlocal thermal equilibrium (NLTE) kinetics model, employing escape factors to approximate the effect of radiative transfer [4,38]. Also included in the theoretical spectra were the effects of ion dynamics and opacity broadening [4], Doppler and instrumental broadening, and ion-quadrupole interactions [20]. The optical depths of the $\beta$ lines are on the order of 1, while optical depths of the $\gamma$ lines are even less. Therefore, opacity broadening has a small effect for the $\beta$ and $\gamma$ lines relative to that experienced by the $\alpha$ lines. In Fig. 4, a typical lineout of spectroscopic data is shown with the ''best fit'' unshifted and shifted theoretical profiles, where only temperature and density are adjustable parameters. We can infer temperature gradients from the presence of Li-like satellites of He $\beta$; however, plasma-induced line shifts are only weakly dependent on temperature. It should be noted that, because the $\alpha$, $\beta$, and $\gamma$ lines shift by significantly different amounts, one *cannot* shift the theoretical spectrum by an arbitrary amount and fit the entire spectrum. In particular, the region containing the Ar He $\gamma$ and Ly $\beta$ lines provides an excellent test of any theory of shifts, as experimental uncertainties are unlikely to vary appreciably over this 200 eV spectral range. Figure 4 illustrates the size of the shift relative to the widths and demonstrates a good agreement of theory to experiment when the shifts are included. Analysis of other implosion experiments produces the same inferences.

## VI. CONCLUSION

We have presented a second-order relaxation model of line broadening, which can be used to produce line shapes for arbitrary highly ionized, multielectron radiators. As a result of employing the full Coulomb expression for the radiator–perturbing-electron interaction, we obtain significant line shifts consistent with previous impact calculations and shifts observed in numerous experiments. In particular, we have observed improvements in the fits of theoretical spectra in comparison with experimental data, especially with regard to the differential shifts within a Rydberg series, as well as asymmetries in individual line profiles. In future work, we plan to apply an all-order, unified model to a broader range of plasma conditions. Considering the impact of the dense plasma line shift on a radiator's level structure, we are currently studying the effect of the shift on mixing between adjacent radiator states along a Rydberg series. Preliminary calculations indicate that the plasma-induced line shifts will have a substantial impact on other aspects of plasma spectroscopy, such as line merging, ionization balance, line-ratio diagnostics, and so forth. We believe that incorporating this shift into a broader picture of plasma physics is necessary and will lead to enhanced analytic capability.

## ACKNOWLEDGMENTS

The research reported in this paper was partially supported by the U.S. Department of Energy Grant Nos. DE-FG03-98SF21525 and DE-FG03-97SF21270 through NLUF.

## APPENDIX: GENERAL TRANSITION ARRAYS

In this appendix, we shall describe in more detail the functions of the operators $D_1$ through $D_7$ shown in Eqs. (27) and (28). More information can be found in Sec. 14-11 of [31].

$D_1$ is a factor arising from coordinate permutations.

$D_2$ arises from coefficient of fractional parentage expansions when the transition involves subshells occupied by more than two electrons.

$D_3$ is a factor arising from the uncoupling of the total spin from the total orbital angular momentum.

$D_4$ is a product of terms arising from the successive uncoupling of orbital angular momenta for subshells included *after* the subshells relevant to the transition.

$D_5$ is a factor arising from *recoupling* the angular momenta and spin of the lower subshell relevant to the transition with its neighboring subshell. Steps 4 and 5 allow the transition to be treated as if the electron moves from a singly occupied subshell to an empty subshell.

$D_6$ arises if the relevant subshells of the transition are not adjacent in the series as the angular momenta are coupled, and it accounts for ''jumping'' over the intervening subshells. The reordering of the subshells involves using a product of Wigner 6-$j$ symbols for each intervening subshell for both orbital angular momentum and spin.

$D_7$ includes the reduced matrix element between the relevent subshells as well as terms to recouple the orbital angular momenta of those subshells to the total orbital angular momenta and to recouple the spins.

[1] L.A. Woltz and C.F. Hooper, Jr., Phys. Rev. A **30**, 468 (1984).

[2] L.A. Woltz and C.F. Hooper, Jr., Phys. Rev. A **38**, 4766 (1988).

[3] R.C. Mancini, D.P. Kilcrease, L.A. Woltz, and C.F. Hooper, Jr., Comput. Phys. Commun. **63**, 314 (1991).

[4] D.A. Haynes, Jr., D.T. Garber, C.F. Hooper, Jr., R.C. Mancini, Y.T. Lee, D.K. Bradley, J. Delettrez, R. Epstein, and P.A. Jaanimagi, Phys. Rev. E **53**, 1042 (1996).

[5] C.F. Hooper, Jr., G.C. Junkel, M.A. Gunderson, D.A. Haynes, Jr., R.C. Mancini, D. Bradley, J. Delettrez, and P. Jaanimagi, in *Strongly Coupled Coulomb Systems*, edited by G. Kalman, J.M. Rommel, and K. Blagoev (Plenum, New York, 1998), p. 385.

[6] Y. Leng, J. Goldhar, H.R. Griem, and R.W. Lee, Phys. Rev. E **52**, 4328 (1995).

[7] O. Renner, P. Sondhauss, D. Salzmann, A. Djaoui, M. Koenig, and E. Förster, J. Quant. Spectrosc. Radiat. Transf. **58**, 851 (1997).

[8] N.C. Woolsey, C.A. Back, R.W. Lee, A. Calisti, C. Mossé, R. Stamm, B. Talin, A. Asfaw, and L.S. Klein, J. Quant. Spectrosc. Radiat. Transf. **65**, 573 (2000).

[9] A. Saemann, K. Eidmann, I.E. Golovkin, R.C. Mancini, E. Andersson, E. Forster, and K. Witte, Phys. Rev. Lett. **82**, 4843 (1999).

[10] H. Nguyen, M. Koenig, D. Benredjem, M. Caby, and G. Coulaud, Phys. Rev. A **33**, 1279 (1986).

[11] M. Koenig, P. Malmoult, and H. Nguyen, Phys. Rev. A **38**, 2089 (1988).
[12] H.R. Griem, M. Blaha, and P.C. Kepple, Phys. Rev. A **41**, 5600 (1990).
[13] H.R. Griem, *Principles of Plasma Spectroscopy* (Cambridge University Press, Cambridge, 1997).
[14] S. Volonté, J. Phys. D **11**, 1615 (1978).
[15] S. Skupsky, Phys. Rev. A **21**, 1316 (1980).
[16] J. Davis and M. Blaha, J. Quant. Spectrosc. Radiat. Transf. **27**, 307 (1982).
[17] X. Yan and S. Ichimaru, Phys. Rev. A **34**, 2173 (1986).
[18] J. Cooper, D.E. Kelleher, and R.W. Lee, in *Proceedings of the 2nd International Conference on the Properties of Hot Dense Matter*, edited by J. Davis, C. Hooper, R. Lee, A. Merts, and B. Rozsnyai (World Scientific Press, Singapore, 1985).
[19] R.W. Lee, J. Quant. Spectrosc. Radiat. Transf. **50**, 561 (1988).
[20] D.P. Kilcrease, R.C. Mancini, and C.F. Hooper, Jr., Phys. Rev. E **48**, 3901 (1993).
[21] D.B. Boercker, C.A. Iglesias, and J.W. Dufty, Phys. Rev. A **36**, 2254 (1987).
[22] B.A. Hammel, C.A. Keane, T.R. Dittrich, D.R. Kania, J.D. Kilkenny, R.W. Lee, and W.K. Levedahl, J. Quant. Spectrosc. Radiat. Transf. **51**, 113 (1994).
[23] C.F. Hooper, Jr., Phys. Rev. **149**, 77 (1966).
[24] E.W. Smith and C.F. Hooper, Jr., Phys. Rev. **157**, 126 (1967).
[25] R.J. Tighe and C.F. Hooper, Jr., Phys. Rev. A **14**, 1514 (1976).
[26] T. Hussey, J. Dufty, and C. Hooper, Phys. Rev. A **12**, 1084 (1975).
[27] J.W. Dufty and D.B. Boercker, J. Quant. Spectrosc. Radiat. Transf. **16**, 1065 (1976).
[28] E. Smith, J. Cooper, and C.R. Vidal, Phys. Rev. **185**, 140 (1969).
[29] R.J. Tighe and C.F. Hooper, Jr., Phys. Rev. A **17**, 410 (1978).
[30] D.B. Boercker and C.A. Iglesias, Phys. Rev. A **30**, 468 (1984).
[31] R.D. Cowan, *The Theory of Atomic Structure and Spectra* (University of California Press, Berkeley, 1981).
[32] C.R. Vidal, J. Cooper, and E. Smith, J. Quant. Spectrosc. Radiat. Transf. **10**, 1011 (1970).
[33] R.L. Greene and J. Cooper, J. Quant. Spectrosc. Radiat. Transf. **15**, 1045 (1975).
[34] M. Gunderson, G. Junkel, D. Haynes, and C. Hooper (unpublished).
[35] M. A. Gunderson, G. C. Junkel, D.A. Haynes, Jr., and C.F. Hooper, Jr. (unpublished).
[36] D.K. Bradley, J.A. Delettrez, R. Epstein, R.P.J. Town, C.P. Verdon, B. Yaakobi, S. Regan, F.J. Marshall, T.R. Boehly, J.P. Knauer, D.D. Meyerhofer, W. Seka, D.A. Haynes, Jr., M. Gunderson, G. Junkel, C.F. Hooper, Jr., P.M. Bell, and T.J. Ognibene, Phys. Plasmas **5**, 1870 (1998).
[37] D.H. Kalantar, P.M. Bell, R.L. Costa, B.A. Hammel, O.L. Landen, T.J. Orzechowski, J.D. Hares, and A.K. Dymoke-Bradshaw, Proc. SPIE **2869**, 680 (1997).
[38] R.C. Mancini, R.F. Joyce, and C.F. Hooper, Jr., J. Phys. B **20**, 1975 (1987).